

Methodological Advances

Cite this article: Feng, J. T., S. Puthanveetil Satheesan, S. Kong, T. H. Donders, and S. W. Punyasena (2025). Addressing the “open world”: detecting and segmenting pollen on palynological slides with deep learning. *Paleobiology*, 1–14.

<https://doi.org/10.1017/pab.2025.10059>

Received: 06 January 2025

Revised: 01 July 2025

Accepted: 15 July 2025


Handling Editor:

Andrew Leslie

Corresponding author:

Surangi W. Punyasena;
Email: spunya1@illinois.edu

Addressing the “open world”: detecting and segmenting pollen on palynological slides with deep learning

Jennifer T. Feng^{1,2}, Sandeep Puthanveetil Satheesan³, Shu Kong⁴,
Timme H. Donders⁵ and Surangi W. Punyasena^{1,3} 

¹Department of Plant Biology, University of Illinois, Urbana, Illinois 61801, U.S.A.

²Department of Anthropology, University of Pennsylvania, Philadelphia, Pennsylvania 19104, U.S.A.

³National Center for Supercomputing Applications, Urbana, Illinois 61801, U.S.A.

⁴Faculty of Science and Technology, University of Macau, Macau 999078, China

⁵Department of Physical Geography, Utrecht University, 3584 CS Utrecht, The Netherlands

Abstract

Fossil pollen analysis is an “open-world” problem in paleontology for which there is a long-standing need for automated identification and classification. In the open world, categorical classes are imbalanced, test classes are not known a priori, and test data are captured across different domains. Pollen samples capture large numbers of specimens that include both common and abundant types and rare and sometimes novel taxa. Pollen is diverse morphologically and features can be altered during fossilization. Additionally, there is little standardization in the imaging of pollen samples. Therefore, generalized workflows for automated pollen analysis require techniques that are robust to these differences and can work with microscope images. We focus on a critical first step, the initial detection of pollen specimens on a palynological slide and review how existing methods can be employed to build robust and generalizable analysis pipelines. First, we demonstrate how a mixture-of-experts approach—the fusion of a general pollen detector with an expert model trained on minority classes—can be used to address taxonomic biases in detections, particularly the missed detections of rarer pollen types. Second, we demonstrate the efficiency of domain fine-tuning in addressing domain gaps—differences in image magnification and resolution across microscopes and of taxa across different sample sources. Third, we demonstrate the importance of continual learning workflows, which integrate expert feedback, in training detection models from incomplete data. Finally, we demonstrate how cutting-edge segmentation models can be used to refine and clean detections for downstream deep learning classification models.

Non-technical Summary

Fossil pollen analysis presents challenges that result from the complexity of the “open world.” It is not possible to anticipate all the taxa that will be encountered in geologic samples. Each sample has the potential to produce new species and introduce specimens with unique shapes and sizes. Pollen embodies diverse morphologies; its appearance can be altered depending on the conditions under which it was fossilized; and there is little standardization in the microscopy equipment used to image and catalog pollen images. AI applications in palynology need to address this complexity. We applied four machine learning methods (mixture-of-expert models, domain fine-tuning, continual learning, and foundation models for segmentation) to fossil pollen data to demonstrate their effectiveness in the detection and isolation of pollen specimens on a pollen sample slide and provide command line software for others to reproduce this work and apply these methods.

Introduction

Fossil pollen analysis represents a paleontological example of an “open-world” problem. The term “open world” describes uncontrolled operational environments in machine learning (Bendale and Boulton 2015; Liu et al. 2019; Joseph et al. 2021). It stands in contrast to classic supervised learning, where all the test classes are known and have been introduced in training. The data collected by pollen analysis—like data from many other fields of paleontology—cannot be fully anticipated and modeled a priori. Specimens often represent new, extinct, and/or undiscovered species. Species abundances (sensu May 1975) naturally follow an imbalanced or long-tailed distribution, where a small number of taxa are common, while many others are rare. Images of the same taxon can vary widely, depending on the microscope, magnification, and imaging or preparation techniques. Specimens can have variable levels of preservation from

© The Author(s), 2025. Published by Cambridge University Press on behalf of Paleontological Society. This is an Open Access article, distributed under the terms of the Creative Commons Attribution licence (<http://creativecommons.org/licenses/by/4.0>), which permits unrestricted re-use, distribution and reproduction, provided the original article is properly cited.

PALEOBIOLOGY
A PUBLICATION OF THE
 **Paleontological SOCIETY**

 **CAMBRIDGE**
UNIVERSITY PRESS

sample to sample and locality to locality. Given the high level of expertise and time required for traditional pollen identifications, researchers have long sought to develop automated detection and classification pipelines for pollen specimens (Langford *et al.* 1990). However, developing machine learning models that can generalize across the range of variability in pollen diversity, abundance, preservation, preparation, and imaging requires adopting workflows that can succeed in open-world environments.

Fossil pollen isolated from geologic sediments for paleoecological or biostratigraphic analysis are typically mounted on microscope slides (Traverse 2007). The first step in any automated classification process is streamlining the imaging of microscopic slides of pollen samples and detecting and segmenting pollen specimens from these scanned images. The widespread availability of slide-scanning microscopes means that entire slides can be imaged quickly and efficiently (Tetard *et al.* 2020; Punyasena *et al.* 2022; Theuerkauf *et al.* 2023; Li *et al.* 2024; von Allmen *et al.* 2024; Jaramillo *et al.* 2025). These scans are capable of capturing the entirety of a pollen slide—both the area of a coverslip and multiple focal planes—producing a fully three-dimensional representation of the pollen sample (Punyasena *et al.* 2022).

Accurate, consistent detection of pollen among other organic debris in these slide scans is a critical step in automating visual pollen identifications. It can be followed by segmentation to isolate the grain from its background. The final step is classification into morphological or taxonomic groupings. While an increasing number of studies have shown that classification is feasible with enough training data (Sevillano and Aznarte 2018; de Geus *et al.* 2019; Menad *et al.* 2019; Astolfi *et al.* 2020; Bourel *et al.* 2020; Sevillano *et al.* 2020; Barnes *et al.* 2023; Rostami *et al.* 2023), training effective detection and segmentation models remains a challenge due to the taxonomic, taphonomic, imaging, and preparation diversity within palynology. Detection in this context refers to the automated location of a pollen specimen within the X, Y, and Z coordinates of a slide scan. Segmentation refers to isolation of the detected specimen from the background. Detection is needed at two discrete stages of automated workflows. Experts can label detected pollen grains to efficiently produce training and validation data for the development of pollen classification models. Detection is also needed when applying these classification models to new samples.

We demonstrate four machine learning solutions for addressing common limitations in automated pollen detection and segmentation. Taken together, these approaches provide effective strategies for constructing robust, generalized detection models that can be applied to a wide range of palynomorphs and other paleobiological data. We first focus on detecting pollen specimens from a scanned image of a microscope slide and demonstrate how the mixture-of-experts technique can address taxonomic bias. The morphological diversity and long tail of rare species encountered in pollen samples, particularly those from the tropics, lead to detectors that are potentially biased toward the most common and distinctive morphological types. False negatives (pollen that is missed by the detector) pose a greater problem than false positives (non-pollen objects identified as pollen by the detector), as false positives can be removed at a later stage of the analysis, while bias toward false negatives will affect downstream estimates of proportional abundance. The solution is to train an expert model on small, difficult-to-detect taxa and fuse it with a more general pollen detector. This technique is used frequently in top-ranked detection methods in

public machine learning challenges (Akiba *et al.* 2018; Guo *et al.* 2019; Huang *et al.* 2020).

We next demonstrate how fine-tuning can be a data-efficient method for transfer learning across new imaging domains. Differences among pollen samples or images result from differences in the microscopes and objectives used, localities or ages represented, or preparation techniques applied. Detection models trained in one domain will have reduced accuracy when applied to a new domain due to differences in color, brightness, and resolution, or the taxonomic or taphonomic differences between samples. Fine-tuning previously trained models with training data from a new domain can quickly produce more generalized models. This approach is widely used in machine learning (for reviews, see Pan and Yang 2010; Zhuang *et al.* 2020).

Next, we show how workflows for continual learning using human-in-the-loop annotation can address the problem of incomplete training data for pollen detection. In fossil pollen analysis, as in many other areas of paleobiological research, there is a high probability of encountering new taxa with each new sample. We inevitably begin with insufficient training data because it is not possible to curate images of all possible types. Incorporating expert feedback through human-in-the-loop annotation leverages trained models to annotate new, unlabeled data. Experts verify or revise low-confidence detections, and these new annotations are used to further fine-tune detection or classification models (Zhou *et al.* 2017; Wang *et al.* 2020; Adhikari and Huttunen 2021; Wu *et al.* 2022; Kirillov *et al.* 2023). This approach provides an efficient mechanism for improving pollen detection (as well as pollen classification) models over time.

Finally, we demonstrate how newly available foundation segmentation models (Meta's Segment Anything Model 2 [SAM-2]; Kirillov *et al.* 2023; Ravi *et al.* 2024) can be incorporated into object detection pipelines of microscope images. Segmentation builds on detection results, producing masked images that follow an object's outline. Cleanly segmented images improve future classification analyses by removing extraneous and potentially biasing information from an image background. The off-the-shelf segmentation model SAM-2 takes a user prompt, for example, a bounding box that specifies a region of interest or a cursor prompt, and outputs a valid segmentation mask. SAM-2 is trained on a segmentation dataset of more than 1 billion masks, 1 million still images, and 51,000 videos, allowing the model to segment general objects of interest on diverse images and videos (Ravi *et al.* 2024).

We review these four foundational and emerging techniques to demonstrate their application to palynological analysis and specifically to the critical first step of pollen detection and segmentation from scanned slide images. Our hope is to encourage and guide other researchers in developing robust deep learning workflows. All Python code used to process slide scans into image stacks, annotate image stacks, train and evaluate detection models, and apply segmentation is available through our GitHub repositories, and we provide command line interface (CLI) Python software so that others can easily integrate these techniques into their own research (see Data Availability Statement). The NDPI Tile Cropper CLI as written can only be applied to Hamamatsu NanoZoomer Digital Pathology Images (NDPI) images (Puthanveetil Satheesan *et al.* 2025a), but the source code shared in our GitHub repository can be modified to open other microscope images using the python-bioformats library, a wrapper for Bio-Formats Open Microscopy Environment software (Linkert *et al.* 2010).

Methods

Pollen Samples Source

We imaged pollen from two high-resolution sediment cores extracted from Laguna Pallcacocha, in El Cajas National Park, Ecuadorian Andes. The first core, PAL 1999, (Moy et al. 2002) extends through the Holocene (11,600 cal yr BP–present). The second parallel core, PAL IV (Hagemans et al. 2021; Hagemans et al. 2023) spans the twentieth century. The vegetation surrounding the lake is dominated by cushion plants and patches of páramo shrubs (Hagemans et al. 2019). Volumetric samples were spiked with *Lycopodium clavatum* and prepared following standing protocols, including acetolysis and heavy liquid flotation (Faegri and Iversen 1989). Samples from PAL IV were mounted using glycerin, and samples from PAL 1999 were mounted in a permanent mount.

Imaging

We imaged 19 slides from the PAL IV core and three slides from the PAL 1999 core using two different microscopes (Fig. 1, Table 1). PAL IV slides were imaged at 630 \times magnification (0.146 μ m/pixel

resolution) with a Leica DM 6000 B, an upright transmitted light microscope fit with a halogen light source, an automated XYZ stage, and LAS 4.12 PowerMosaic software for the creation of image tile grids (Fig. 1B). One to three scans measuring 3698 μ m \times 2790 μ m were taken from each slide. Each scan was composed of 400 image stacks of 1040 \times 1392 pixel tiles, with 7 or 9 focal planes imaged at increments of 3 or 4 μ m. A total of 2986 image stacks contained palynomorphs; these were used for model training. The three samples from the PAL 1999 core were imaged at 400 \times magnification (0.225 μ m/pixel resolution) with a Hamamatsu NanoZoomer 2.0 HT slide-scanning microscope. Nine focal planes were imaged in 3 μ m increments for a focal depth range of 24 μ m. Slide scans (NDPI file format) were processed into 1040 \times 1392 pixel image stacks (PNG file format) using the Bio-Formats Python library (Linkert et al. 2010). Three hundred randomly selected image stacks, approximately 5% of the total slide area, were exported from each slide.

Annotation

For every annotated pollen grain or spore, we defined its X,Y,Z coordinates using bounding boxes converted to inscribed circles

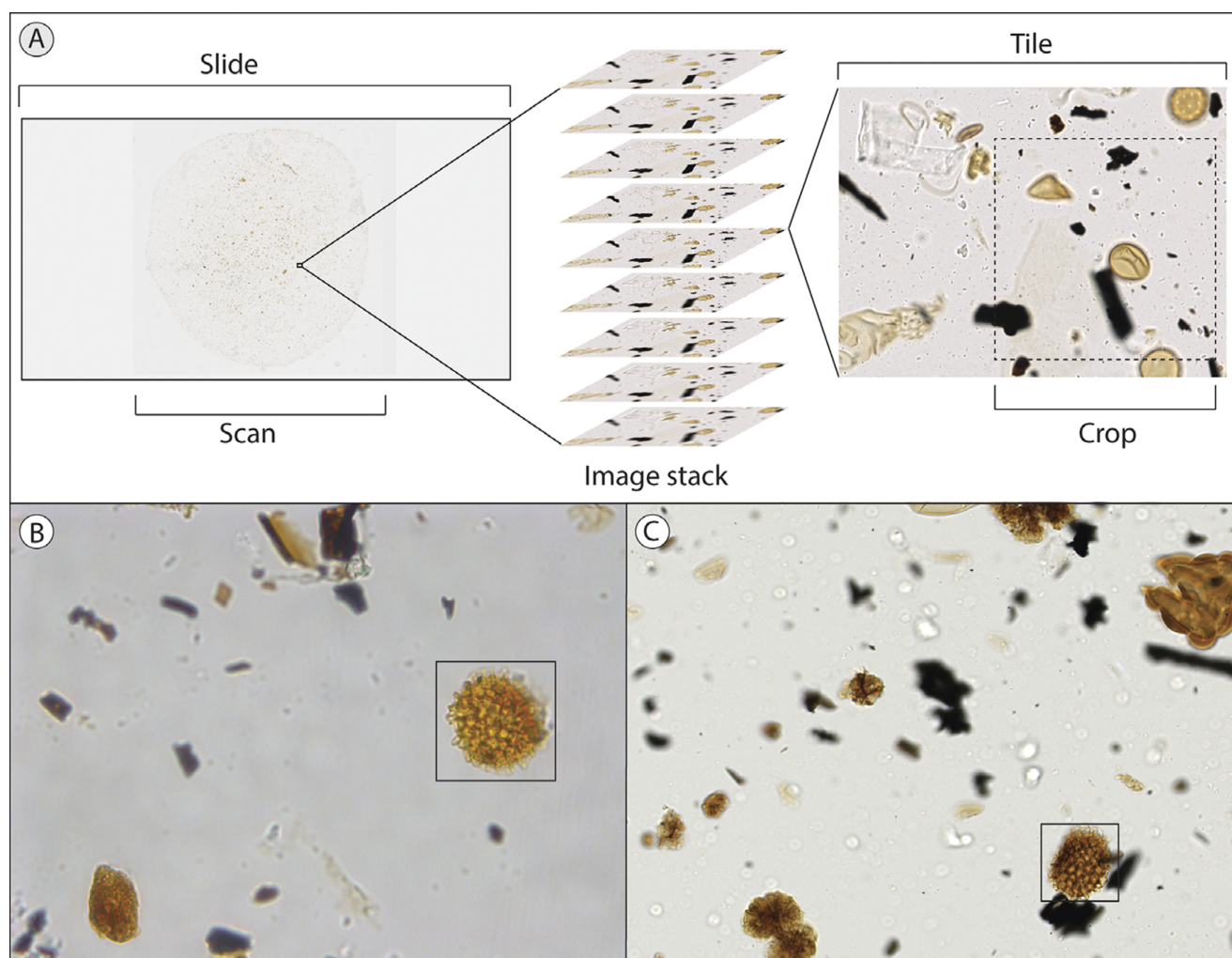


Figure 1. A, Example of a slide scan (~20.5 \times 20.5 mm), image stack (7 or 9 focal planes with 3 or 4 μ m step size), image tile (1040 \times 1392 pixels), and crop (800 \times 800 pixels). Comparison of 1040 \times 1392 pixel image tiles taken with a (B) standard upright microscope (0.146 μ m/pixel) and (C) slide-scanning microscope (0.225 μ m/pixel). The 40 \times 40 μ m boxes highlight *Lycopodium* spores in each image for comparison. Noticeable differences include color, brightness, and scale. The upright microscope domain was used in training the general pollen detection model (GPDM) and small-grain detection model (SGDM), and the slide-scanning microscope domain was used for domain fine-tuning and continual learning.

Table 1. Summary of the two different slide imaging and image tiling methods used in this paper, identifying several variables: the sediment core source for the pollen sample, the techniques described in the paper used on those samples, the number of slides used in the analysis, the microscope used for imaging, the lens magnification and image resolution, the number of focal planes in the image stacks, the image stack focal plane step size, the focal depth range of the image stack, the slide image tiling method, and the tile dimensions. Samples were imaged using two different but comparable bright-field microscopy methods, making use of the available institutional resources at Utrecht University and the University of Illinois, Urbana-Champaign. GPDM, general pollen detection model

Sediment core	PAL IV (Hagemans et al. 2021, 2023) spans the twentieth century	PAL 1999 (Moy et al. 2002) spans the Holocene
Relevant methods	Training GPDM, mixture-of-experts approach	Transfer learning and human-in-the-loop approaches
Number of slides	19	3
Microscope	Leica DM 6000 B, upright transmitted light microscope	NanoZoomer 2.0 HT slide scanning microscope
Lens magnification and image resolution	630× (0.146 μm/pixel)	400× (0.225 μm/pixel)
Number of focal planes	7 or 9	9
Image stack step size	3 or 4 μm	4 μm
Focal depth range of image stack	24 μm	24 μm
Image tiling method	Microscope fitted with an automated XYZ stage and LAS 4.12 PowerMosaic software for the creation of image tile grids (BMP format)	Whole slide scans (NDPI format) processed into tiles (PNG format) using the Bio-Formats Python library
Tile dimensions	1040 × 1392 pixels	1040 × 1392 pixels

(PAL IV images) or directly as circles (PAL 1999 images) on the plane of the image stack that captured the equatorial cross section of the pollen grain or spore. When these annotations fell at the edge of the image, annotations were corrected manually to identify the center of the grain. We annotated the PAL IV images using a MATLAB script, modified from Punyasena et al. (2022), and annotated the PAL 1999 images using Labelme (Wada et al. 2021) and the Hamamatsu NanoZoomer NDP.view2 software. All three methods produced the same annotation metadata: a center and radius that defined the location of a pollen grain. We annotated 3191 PAL IV and 794 PAL 1999 specimens as one of 129 taxonomic types (Feng et al. 2025). The 18 most common palynomorphs accounted for 92% of the total dataset (Fig. 2). We excluded algae and fungal spores, but included plant spores from ferns and lycopods, such as *Huperzia* (Fig. 2P), *Isoetes* (Fig. 2Q), and the exote marker *Lycopodium clavatum* (Fig. 2R). The excluded algae were primarily *Pediastrum*, which is much larger and lighter than pollen and morphologically distinct. Similarly, the excluded fungal spores are much smaller and darker than pollen and likewise morphologically distinct.

General Pollen Detection Model (GPDM) Architecture and Training

Convolutional neural networks (CNNs) have learnable parameters that are optimized to output the desired prediction for a given input. A CNN model is trained using a set of images and their associated annotations. Annotations refer to human expert labels or tags of specimens and their bounding box coordinates. This is the “ground truth.” From the training set, a random selection of images is forward passed through the model, which outputs detection results. The detection results are compared with the ground-truth annotations of these images, producing a loss that measures the difference between detection results and annotations. Then, an optimization algorithm updates the model’s parameters by minimizing the cost value. This procedure iterates over batches of the whole training data, for multiple epochs (where an epoch is a single pass over all the training data). Intermediate models are saved after each

epoch or saved under different training hyperparameters, and we select the model that produces the smallest cost value on a held-out validation set (Fig. 3A).

In our case, our input is image stacks from slide scans, and our desired prediction is pollen detections (determining whether image pixels represent “pollen” or “not pollen”). We used ResNet34 (He et al. 2016) as the backbone of our GPDM, encoding the input image stacks as a feature map, which assembles per-pixel feature vectors. Over the feature map, we built a decoder (Kong 2022; Punyasena et al. 2022) that transformed the feature map to a detection heat map, with each pixel denoting a confidence score for the pixel belonging to a pollen grain.

We used the PAL IV dataset in developing the GPDM. The model was trained on 800 × 800 pixel crops of the original 1040 × 1392 pixel image tiles (Fig. 1A). During training, crops were taken randomly, and the location of the crop varied with each epoch. During evaluation, four overlapping crops were taken of each image stack, covering the entire image tile. We divided the annotated image stacks into a training set (80%) and a validation set (20%). We augmented the training data using random rotations and flips of the original image stacks. We set the number of images in each batch of training data to four, trained the model for 30 epochs, and set the learning rate (the degree of model weight adjustment for each weight update) to 0.0005. We stopped the training at 30 epochs when the model improvement plateaued.

We created circular binary masks to indicate where pollen was present using our circular annotations. From these, we created distance transform masks where values for pixels inside each circle or partial circle represented the number of pixels to the nearest edge (Fig. 4B). Binary masks were used to train the model to recognize pixels in an image as “pollen” or “not pollen,” while the distance transform masks were used to train the model to recognize the centers of pollen grains. Use of the distance transform masks creates a spatially aware detection, allowing for the separation of overlapping detections and cleaner segmentations (e.g., Punyasena et al. 2022). The final loss sums the detection loss and the distance transform loss.

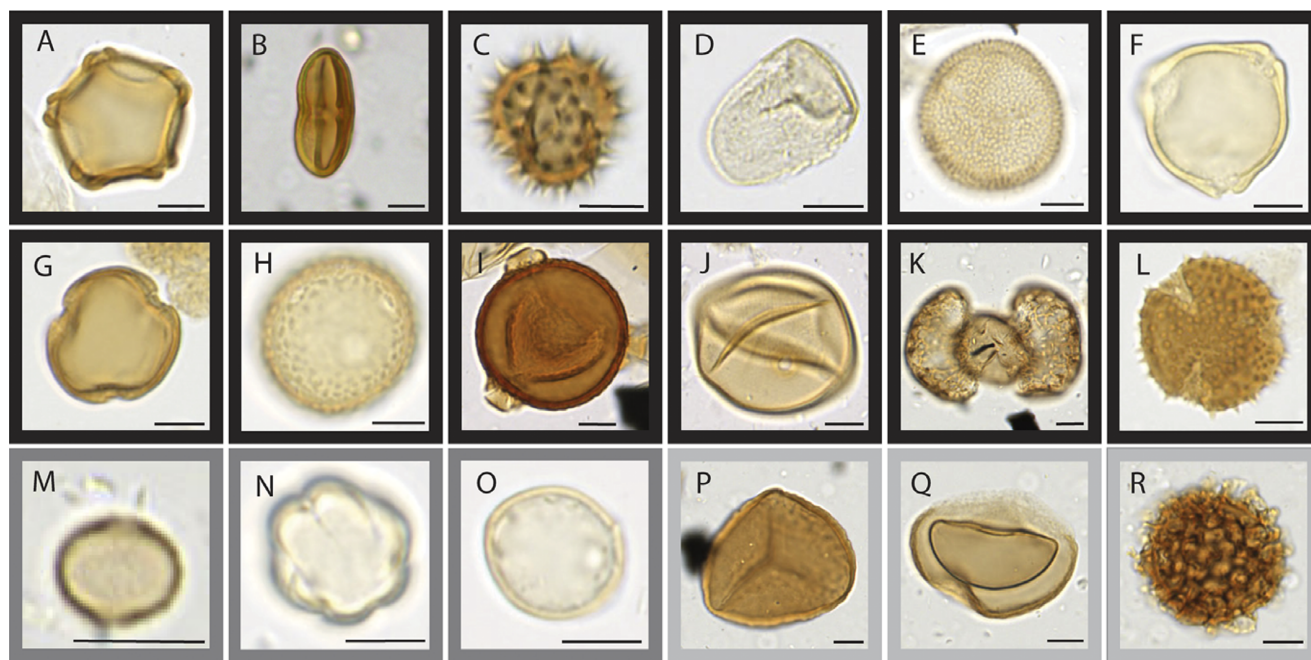


Figure 2. The 18 most common palynomorphs (>20 training examples, representing 92% of the total dataset): **A**, *Alnus*; **B**, Apiaceae; **C**, Asteraceae Tubuliflorae-type; **D**, Cyperaceae; **E**, *Hedyosmum*; **F**, *Myrica*; **G**, *Myrsine*; **H**, *Plantago*; **I**, *Polylepis* spp.; **J**, Poaceae; **K**, *Podocarpus*; **L**, *Valeriana*; **N**, *Cecropia*; **M**, Melastomataceae; **O**, Urticaceae-Moraceae; **P**, *Huperzia*; **Q**, *Isoetes*; and **R**, *Lycopodium clavatum* (exote marker). Black borders indicate taxa with medium to large pollen grains (**A–L**), medium-gray borders indicate taxa with small grains (**M–O**), and light gray borders indicate plant spores included in the annotated dataset (**P–R**). Scale bars, 10 μm .

Detection Model Outputs

For each image in an image stack, the detection model outputs softmax layers (normally distributed probabilities of whether a pixel is within a pollen grain) (Fig. 4C) and predicted distance transform layers of pollen pixels from the edge of a pollen grain (Fig. 4D). Local peaks in the distance transform layer identified the mass centers of pollen detections (Fig. 4E). We next used the maximum radius of the largest connected component as the predicted radius. The predicted center and radius defined the circular binary detection mask (Fig. 4F). Softmax was used to determine the confidence of the detection (Punyasena et al. 2022).

Detection Model Evaluation

We evaluated detections by determining the overlap with the closest annotated pollen grain (Fig. 4A) using their intersection over union (IoU) (Padilla et al. 2021). If an IoU was above a predefined IoU threshold (heuristically chosen as 0.3 for this study, or an overlap of 30%), the detection was considered as a true positive (Fig. 4F), otherwise it was a false positive. If an annotation did not overlap with any detections above the IoU threshold, it was considered a false negative. IoU values of true positives were consistently lower than 1, because the masks defined by machine detections and human annotations were rarely the same size and shape.

We used confidence scores to rank all the detections. Increasing the confidence threshold keeps only high-confidence detections but removes true positive detections with lower confidence. It also potentially increases the percentage of true positives in the retained detections. Therefore, tuning the confidence threshold introduces a trade-off between the percentage of kept true positives over all annotations (termed “recall”) and the percentage of kept true positives over the kept detections (termed “precision”). We define precision and recall, respectively:

$$\text{precision} = \frac{\text{true positives}}{\text{true positives} + \text{false positives}} \quad (1)$$

$$\text{recall} = \frac{\text{true positives}}{\text{true positives} + \text{false negatives}} \quad (2)$$

We calculated the values for precision and recall at varying confidence thresholds and plotted a precision–recall curve from these results. The area under the curve is the mean average precision (mAP), which we can then use to evaluate model performance (Everingham et al. 2010; Lin et al. 2014). Within an image stack, there may be multiple detections for the same grain. We used non-maximum suppression to remove duplicates when the IoU of two detections was ≥ 0.3 , retaining only the detection with the highest confidence score.

Mixture-of-Experts

In our samples, small grains (<20 μm in diameter) were only 6.8% of the total dataset, so taxonomic bias in the data distribution included a morphological bias against the detection of small grains. We used an expert model trained specifically on smaller pollen grains (a small-grain detection model [SGDM]) alongside GPDM detections to improve our detection results (Fig. 3B). This is known as a mixture-of-experts approach (Nowlan and Hinton 1990).

We fine-tuned the GPDM exclusively on three small-grained taxa: Urticaceae-Moraceae (132 image stacks for training and 32 for validation, with each image stack representing a single pollen grain), *Cecropia* (19 training/4 validation), and Melastomataceae (25 training/4 validation). The fine-tuned model is our SGDM. We fine-tuned the SGDM for 80 epochs. (We needed more epochs to train the SGDM than the GPDM due to the greater challenge of learning to detect smaller grains from high-resolution tiles). We

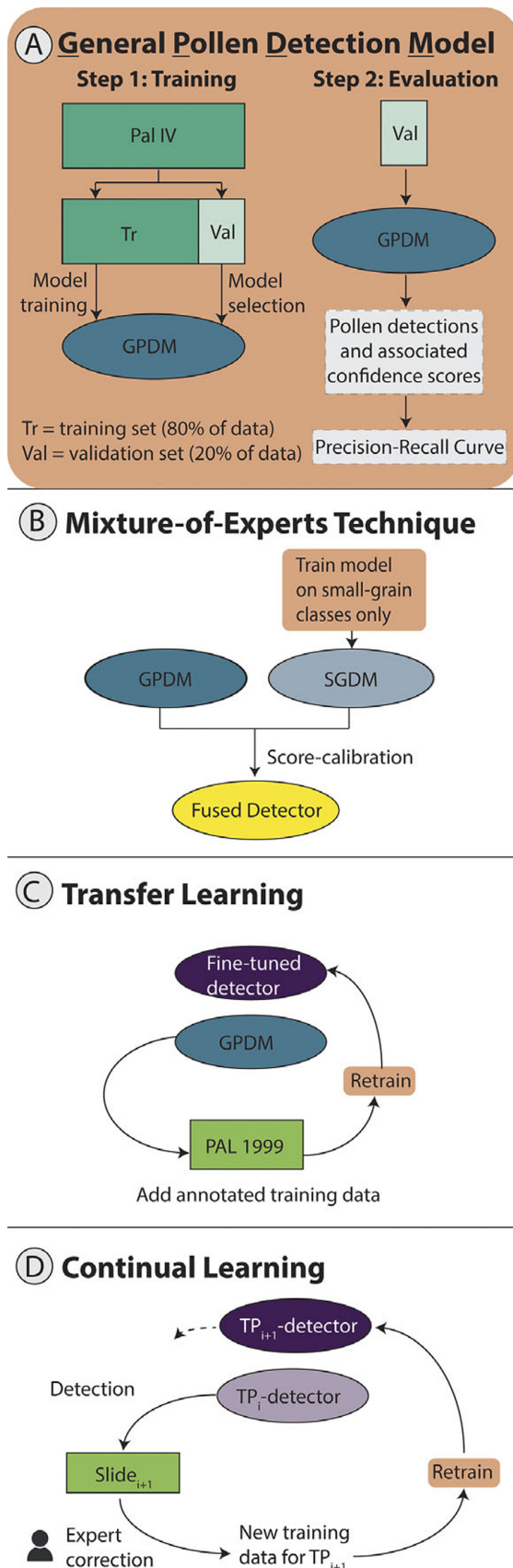


Figure 3. Setups for: **A**, the general pollen detection model (GPDM), **B**, the mixture-of-experts technique, **C**, transfer learning across imaging domains, and **D**, continual learning with human-in-the-loop annotation. **A**, The process of training the GPDM by

splitting the annotated dataset into training and validation sets, used respectively for training the model and for model selection. The validation set was then passed through the model to obtain a list of detections and associated confidence scores. Using the detections, we drew a precision–recall curve for model evaluation. **B–D** are variations on **A**. In **B**, we trained a small-grain detection model (SGDM) on a subset of the PAL IV data, selecting only image stacks that contained Urticaceae-Moraceae, Melastomataceae, or *Cecropia* grains and revising the masks to only represent these taxa. The SGDM was then fused with the GPDM into a single pipeline. In **C**, we fine-tuned the GPDM on slides from a new domain, PAL 1999. In **D**, we implemented a continual learning workflow. We used Slide 1 to fine-tune the GPDM in TP₀, producing the TP₁ detector, then used the TP₁ detector to detect pollen in image stacks from Slide 2. In the fine-tuning stage, experts manually verified detections so that the detections served as new training data to fine-tune detectors. The process was repeated continually in subsequent time steps.

reserved examples from three other small-grained taxa—*Acalypha*, *Vallea*, and *Weinmannia*—as a held-out validation set to assess the ability of SGDM to detect novel taxa with similar characteristics. We used this validation set to evaluate both SGDM and GPDM in terms of detecting small pollen grains.

The SGDM and GPDM produced independent sets of detections with different confidence score distributions. To fuse their detections, we first calibrated their confidence scores using the method in Platt (1999) for score calibration. Specifically, we adjusted the confidence score (s) of an SGDM's detection towards the calibrated score (S) by tuning two hyperparameters (α and β) in the sigmoid function below:

$$S = \frac{1}{1 + e^{-S * \alpha + \beta}} \quad (3)$$

We tuned the hyperparameters by sweeping over a range (3.0, 6.0) for α and β , with step sizes of 0.1, with a goal of maximizing mAP over our validation set. We derived the final hyperparameter at $\alpha = 5.5$ and $\beta = 4.9$ used in our work. We fused overlapping detections from the GPDM and SGDM.

Transfer Learning across Imaging Domains

We next fine-tuned our GPDM, originally trained on PAL IV images, to new imaging domains, that is, the PAL 1999 images. Because the taxonomic composition of the two cores was identical, differences between the two image datasets were primarily in the image resolution, color, and contrast (Hagemans et al. 2022, 2023). The PAL 1999 dataset included 300 image stacks from each of three slides; 80% were used as the training set and 20% as the validation set. The GPDM was trained on PAL 1999 image stacks and annotations (Fig. 3C), until we observed no additional model improvement (120 epochs). Although the PAL IV images had a resolution of 0.146 $\mu\text{m}/\text{pixel}$ and PAL 1999 images had a resolution of 0.225 $\mu\text{m}/\text{pixel}$, we did not rescale the images to simulate a more challenging domain gap. We evaluated the fine-tuned model performance by comparing the precision–recall curves for the slide-scanner validation data before and after fine-tuning. To provide a performance baseline for comparison, we also trained a GPDM model trained from scratch on the PAL 1999 image stacks and annotations.

Continual Learning with Human-in-the-Loop

We simulated a human-in-the-loop workflow that would allow us to train models when starting with incomplete data. Instead of training on all 900 images at once as in our transfer learning experiments, we split the images at the slide level into three sets of training and validation data to be used at three time periods (TP₀, TP₁, and TP₂). We measured model performance as the decrease in

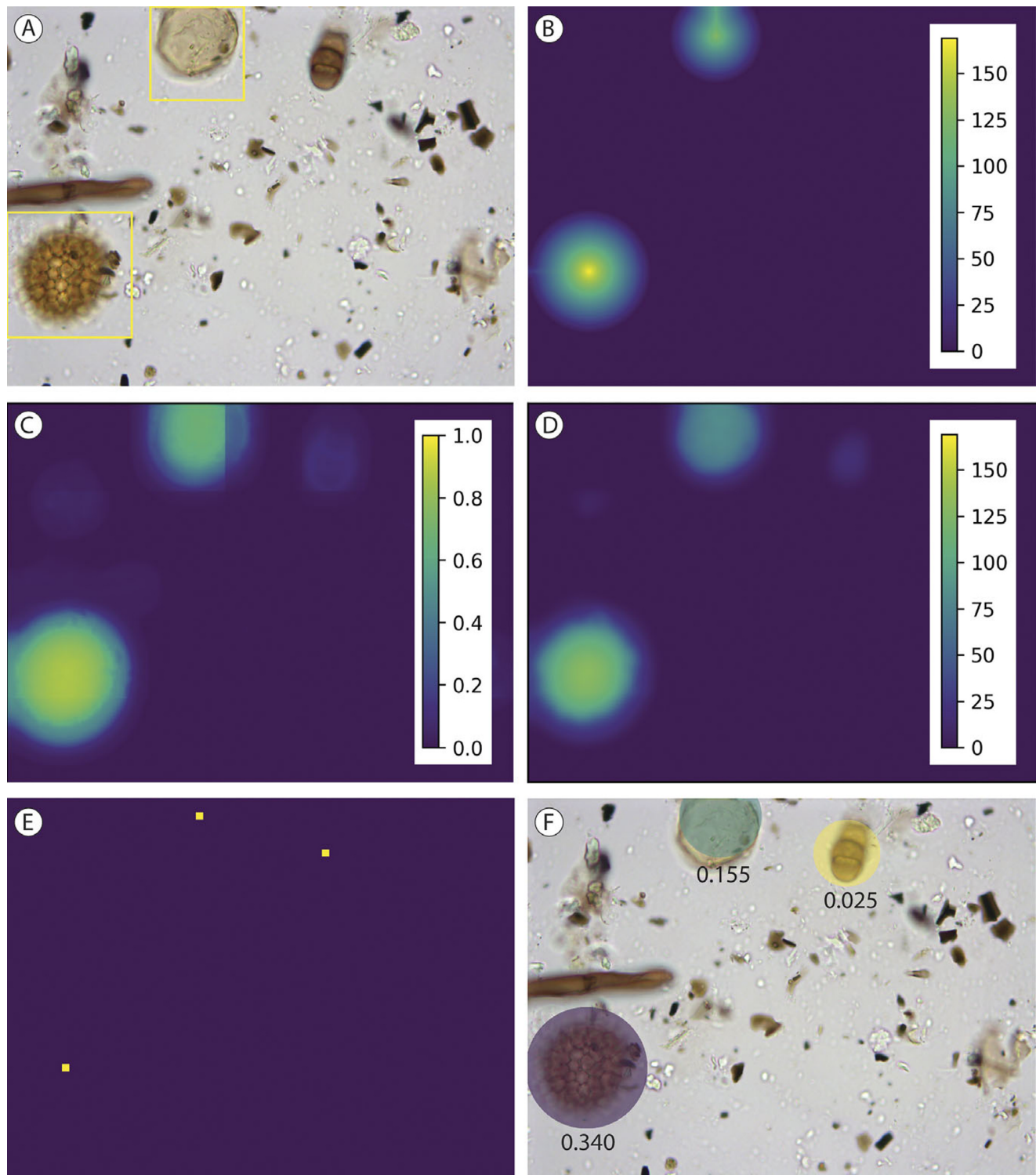


Figure 4. The detection workflow. **A**, One plane of the image stack, overlaid with the original square annotations. **B**, The ground-truth distance transform mask, created from the annotations. **C**, The softmax layer, one of the model outputs. **D**, The predicted distance transform mask, a second model output. **E**, The predicted pollen grain centers, determined by calculating the peaks in the distance transform mask. **F**, The detection mask, created using the predicted pollen grain centers and radii, overlaid on the image with confidence scores below each detection. The detection mask was thresholded at a confidence score of 0.025. Note that a single image is used solely to illustrate our workflow. In our study, training and evaluation images were not duplicated.

the number of false positives and an increase in the recall rate. We manually verified true positives and false positives in our detection results from each time period and used these new labels to further fine-tune our models (Fig. 3D).

In TP_0 , we fine-tuned the GPDM on the TP_0 training set and used the TP_0 validation set to select the best-performing detector, which we called the TP_0 detector. In TP_1 , we used the TP_0 detector to help us annotate the TP_1 training set. We ran the TP_0 detector on

the TP₁ training set to get a set of detections. Next, we simulated human-in-the-loop verification of the detections by using the ground-truth annotations. If a ground-truth annotation and a predicted detection had an IoU > 0.3, we considered the detection a true positive and included it in the set of cleaned annotations for the TP₁ training set. Otherwise, the detection was considered a false positive and was eliminated. We did not include missed detections in the cleaned annotations for the TP₁ training set. We fine-tuned the TP₀ detector on a training set composed of [TP₀ training set + TP₁ training set] and selected the best model using the TP₁ validation set. We called this detector the TP₁ detector. In TP₂, we repeated the process of using the TP₁ detector to annotate the current TP₂ training set, then cleaning up the annotations. We fine-tuned the TP₁ detector on a training set composed of [TP₀ training set + TP₁ training set + TP₂ training set] and selected the best model using the TP₂ validation set. We called this detector the TP₂ detector.

Zero-Shot Segmentation

The shape of a pollen grain outline varies with orientation, preservation, and species morphology. Not all pollen grains are circular in cross section. As a result, circular detection masks can include extraneous background material, such as organic debris or adjacent grains. Equally, portions of the grain can be excluded when pollen shape deviates significantly from circular. New foundation segmentation models like SAM-2 allow segmentation of pollen grains without needing pollen images to fine-tune, that is, “zero-shot segmentation” (Ravi et al. 2024). To evaluate the efficacy of SAM-2 with palynological images, we applied it to our pollen detections to produce more-contoured segmentation masks that followed the true outlines of detected grains. We used the pollen grain center and the cropped pollen image output by our detection models as input for SAM-2. We also experimented with adding four points near the four corners of the detection mask as negative prompts to SAM-2 to unambiguously differentiate foreground from the background.

Workflow Modules Development, Deployment, and Testing

Finally, we developed CLIs of the individual modules of the pollen analysis workflow described in this paper to allow others to reproduce the analysis and adopt the image extraction and detection workflows (listed in the Data Availability Statement). Written in Python, the CLIs are for tile cropping Hamamatsu NDPI, running trained pollen image detection models, and post-processing with SAM-2 segmentation. The NDPI Tile Cropper CLI is written specifically for opening and processing NDPI images, but can be modified to open other microscope images.

There are several advantages to employing the CLIs. These include the ability to: switch between running in serial and parallel mode; install and manage dependencies using Docker or Apptainer software on high-performance computing (HPC) systems; access optional parameters; and produce user feedback logs. We developed, deployed, and tested the CLIs using different computing environments (e.g., laptop, HPC, and cloud computing) and provide detailed documentation on installation and usage in our GitHub repositories (Puthanveetil Satheesan et al. 2025a,b,c; see Data Availability Statement).

Results

GPDM

We achieved a maximum detection recall rate of 93% and mAP of 73.21% with the full PAL IV image dataset (Fig. 5A). We set the

threshold for the desired precision of our model output to 20% to remove the majority of false detections. At 20% precision, we achieved ~90% recall across our experiments. The GPDM under-detected smaller, more transparent pollen grains such as Urticaceae-Moraceae, *Cecropia*, Melastomataceae, *Acalypha*, *Vallea*, and *Weinmannia* (Fig. 5C). For example, although *Cecropia* was a more common pollen type, with 19 training examples (Fig. 2M), none of the four images in the validation set were detected at the 20% precision level. In contrast, the larger and darker grains of *Polylepis* spp. (Fig. 2I), of which there were also 19 training examples, had 100% recall.

Mixture-of-Experts Technique

Fusing the SGDM with the GPDM increased maximum recall by 2% and increased mAP from 73.21% to 75.09% (Fig. 5A). Recall at the 20% precision level increased for Urticaceae-Moraceae from 69% to 81%, Melastomataceae from 75% to 100%, and *Cecropia* from 0% to 50% (Fig. 5C). *Acalypha*, *Vallea*, and *Weinmannia*, the three remaining taxa with small, transparent pollen grains, also showed improvement, despite not being included as SGDM training examples (Fig. 5C). The fused SGDM + GPDM model shows an increase in model precision within a large range of recall in (0.1, 0.9), indicating that the SGDM added some high-confidence small-pollen detections (Fig. 5A). The increase in maximum recall shows that the SGDM added detections that are missed by the GPDM (Fig. 5A,B).

Transfer Learning across Imaging Domains

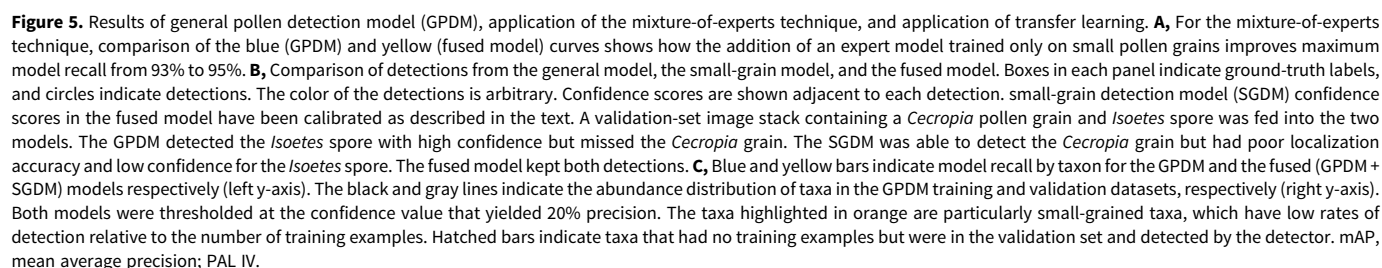
We achieved a mAP of 32.56%, maximum recall of 82%, and 10% precision at the 80% recall level when we forward-passed the PAL 1999 (slide-scanner) images through the GPDM trained on PAL IV (upright microscope) images. The low performance demonstrated the extent to which the detection models were sensitive to domain differences caused by illumination, optical resolution, and camera property offsets. After fine-tuning the model with 900 PAL 1999 training images, we achieved a mAP of 65.99% and precision increased from 10% to 46% at the 80% recall level (Fig. 6). Maximum recall increased from 82% to 93%. The model trained from scratch on the 900 PAL 1999 images achieved a mAP of only 59.27% (Fig. 6).

Continual Learning with Human-in-the-Loop

Human-in-the-loop fine-tuning increased mAP with each iteration, from 34.11% to 58.72% in TP₀, from 48.25% to 62.60% in TP₁, and from 61.57% to 76.01% in TP₂ (Fig. 7). To compare model performance across all three time periods, we also evaluated each model on a common validation set (composed of the TP₀ + TP₁ + TP₂ validation sets). Against this common validation set, mAP increased from 41.10% with the TP₀ model to 59.93% using the TP₂ model (Fig. 7D).

Zero-Shot Segmentation

The SAM-2 segmentation masks with the highest probability scores closely followed pollen grain shape (Fig. 8). We used a single point, the center of the original detection bounding box, to prompt SAM-2. Because the detection bounding box tightly bounds the detection, the center of the detection mask identified the region of interest and provided a clean input prompt for SAM-2. Adding four



recognize nearly the entirety of a pollen grain, although the foundation model had not been trained on pollen images. To completely capture the pollen wall, we applied dilation (an image processing morphological operation; 5×5 kernel over 1 iteration) to expand the area captured by the segmentation mask and ensure

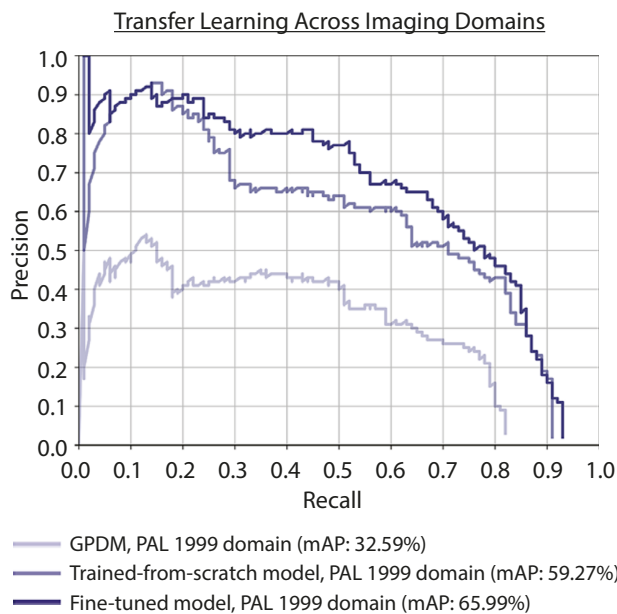


Figure 6. Comparison of the lightest and darkest purple curves shows the improvement of the model after fine-tuning. Maximum recall increased from 82% to 93% and precision increased from 10% to 46% at the 80% recall level. The medium purple curve, representing the performance of a model trained from scratch on the PAL 1999 domain, shows that training from scratch on a small dataset is not as effective as fine-tuning.

that the mask completely captured the pollen wall and external ornamentation.

Discussion

Rapid slide imaging is possible with the commercial availability of automated stages and slide-scanning microscopes (e.g., Punyasena et al. 2022; Theuerkauf et al. 2023). Efficient object detection in scanned slide images will streamline the process of annotating and curating training data, and effective generalized detectors will lower barriers to the adoption of machine learning in palynology and other fields of microfossil research.

Several studies have developed detection and classification methods for analyzing environmental pollen on slides (e.g., Battiatto et al. 2020; Kubera et al. 2022; Punyasena et al. 2022; Tešendić et al. 2022; Gimenez et al. 2024; Li et al. 2024; for a review, see Buters et al. 2022), and instruments for detecting and classifying airborne pollen are commercially available (Oteros et al. 2020). Additionally, imaging flow cytometry can process particles rapidly, and some instruments are capable of simultaneously taking bright-field and fluorescence images of particles. The autofluorescence of pollen grains are used to visually isolate them (Dunker et al. 2021; Barnes et al. 2023).

However, fossil pollen detection presents its own unique challenges. Pollen morphology is altered by the processes of fossilization, which introduce taphonomic artifacts and morphological distortions that vary with taxonomic composition and depositional environments (Cushing 1967; Delcourt and Delcourt 1980; Campbell 1999). Fossil samples may also contain more inorganic sediment, a larger number of unknown plant taxa, and a greater diversity of non-pollen organic debris, all of which introduce noise to automated analyses. Most fossil pollen material is mounted on slides. Automated detection methods compatible with traditional counting and archival material rely on scanning

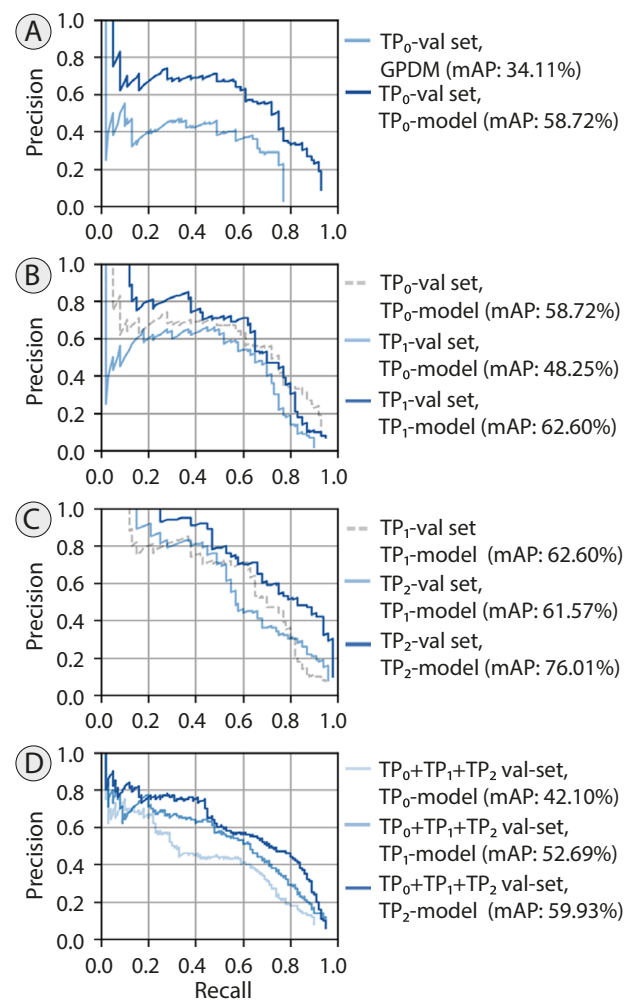


Figure 7. A–C, The improvement in model performance from fine-tuning in three time periods. **A,** The light blue curve represents the performance of the general pollen detection model (GPDM) on the TP₀ validation set. The darker blue line shows the increase in model performance after fine-tuning on the TP₀ training set with ground-truth annotations. **B,** The second time step, TP₁. The dashed gray curve is the same as the dark blue curve in **A**. Comparing the dashed gray curve with the light blue curve shows the drop in model performance when switching slides and introducing a domain gap. Comparing the light and dark blue curves, we see that fine-tuning on the expert-verified TP₀ model detections of the TP₁ training set improves model performance again. **C,** A similar pattern is shown in the next time step, TP₂. **D,** A comparison of the performance of the three models on the same validation set. Here, the TP₀ + TP₁ + TP₂ validation set. mAP, mean average precision.

slides using multiple focal planes (12 to 5 planes, spaced <3 to 8 μ m; Theuerkauf et al. 2023; Gimenez et al. 2024; von Allmen et al. 2024).

While previous studies fused the sharpest portions of the image stacks into a single 2D image using focus stacking algorithms, the detection model described in our analysis is trained directly on unfused image stacks. This approach retains the spatial information contained in all focal planes and allows post hoc selection of the most in-focus plane or the entire image stack for downstream analyses. We use the mAP metric to evaluate and benchmark model performance because it is agnostic to IoU and confidence thresholds. That is, at different IoU and confidence thresholds, recall and precision will differ, but by using precision–recall curves, we can evaluate the relationship between the two metrics at all confidence thresholds. The confidence threshold can be set by the user

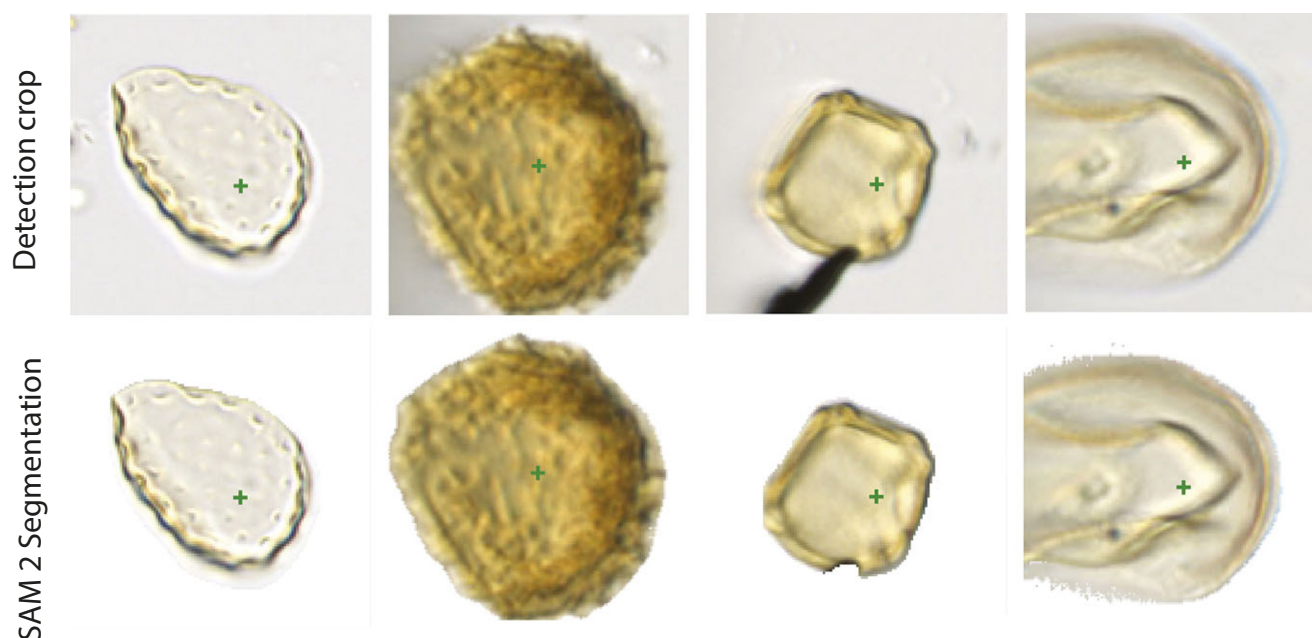


Figure 8. Illustration of segmentation of cropped and detected pollen images using Segment Anything Model 2 (SAM-2). Top row shows the cropped pollen grain images produced by our U-Net convolutional neural networks (CNN) pollen detection model. Taxon identifications from left to right: Amaranthaceae, *Lycopodium*, *Alnus*, Poaceae. Bottom row shows the grain segmented with SAM-2 using an input prompt. The prompt is generated by the detection model and is illustrated with a small green cross.

depending on the application. In most cases, a high recall rate is preferable, because false detections can be further eliminated during classification or manual post-processing (Theuerkauf et al. 2023; von Allmen et al. 2024).

The choice of CNN architecture can vary. We used ResNet34 (He et al. 2016). Von Allmen et al. (2024) used CenterNet Hourglass104 (Duan et al. 2019). Theuerkauf et al. (2023) used Faster R-CNN (Ren et al. 2016). Gimenez et al. (2024) used the joint detection and classification model YOLOv5 (Zhang et al. 2022). These previous studies achieved detection accuracies >90%, but with a limited number of taxa (10 to 11 pollen types). They demonstrate that while high recall rates are possible within a small number of taxa, the diversity and long-tail distribution of pollen taxa within paleontological samples makes detecting rare and unusual morphotypes difficult. Theuerkauf et al. (2023) addressed this imbalance by undersampling majority classes and von Allmen et al. (2024) by selectively balancing training data.

We also found that the GPDM underdetected taxa with small, transparent grains: Urticaceae-Moraceae, *Cecropia*, Melastomataceae, *Acalypha*, *Vallea*, and *Weinmannia* (Fig. 5C). These smaller-grained taxa were not only rare but also differed morphologically from the majority of the training data. In contrast, rare taxa that were similar in size, shape, and color to taxa in the training set were easily detected by the GPDM. For example, Ericaceae, *Rumex*, and *Lupine* were detected with 100% recall in the test set (Fig. 5C), despite having 10 or fewer training examples.

The mixture-of-experts technique (Nowlan and Hinton 1990) allowed us to address taxonomic bias without additional annotated data. Fusing an expert SGDM with the GPDM increased detections of rare, small-grained taxa. Three taxa that were not included as SGDM training examples (*Acalypha*, *Vallea*, and *Weinmannia*) also showed improvement (Fig. 5C). This suggests that the SGDM-learned features were transferable across taxa with similar morphologies. However, taxa with few training examples can still be missed stochastically based on which images are included in

training and validation. For example, two rarer taxa, Loranthaceae and *Thalictrum*, were entirely missed by both the GPDM and SGDM (Fig. 5C). At 20% precision, we achieved ~90% recall across our experiments. Lowering the precision threshold increased detections and recall but introduced a greater percentage of false detections. Threshold selection, therefore, is ultimately dependent on the application and tolerance for missed versus false detections and will likely need to be determined on a case-by-case basis. Previous work has demonstrated that the abundance of a particular pollen taxon, the abundance of a particular pollen morphology, and the degree of morphological similarity to organic debris all contribute to detection errors (Theuerkauf et al. 2023; Gimenez et al. 2024).

Including reference specimens in model training is a potential solution to increasing the taxonomic diversity represented within detection and classification models. Barnes et al. (2023) successfully applied classification models trained on images of modern pollen samples acquired using imaging flow cytometry to fossil material. However, Durand et al. (2024) found that differences in the preservation quality and processing of fresh reference specimens limited the model generalizability to fossil pollen analysis.

Differences in sample preparation and imaging practices create domain gaps among image datasets. Previous work has shown that transfer learning is effective in pollen classification (Rostami et al. 2023; von Allmen et al. 2024), and we demonstrate that transfer learning is also effective in the context of detection. This allows us to deal with domain gaps introduced by different microscope models and scanning conditions. Detection models need to work with multiple imaging sources, as standardizing imaging across large imaging projects is not always feasible, manual annotations are costly in terms of expert time, and training new models for every dataset is not always possible. However, it is possible to fine-tune pretrained detection models on relatively small amounts of training data from new imaging domains. We needed to annotate only 5% of images from a new imaging and sampling domain to increase mAP from 32.56% to 65.99% (Fig. 6), while training

from scratch on the new domain alone achieved a mAP of 59.27% (Fig. 6).

Collaboration between institutions with different microscopes and imaging equipment is therefore a feasible (and potentially desirable) approach, as diverse training data will aid in the development of large, robust pollen analysis pipelines. The creation and maintenance of accessible and discoverable image databases and adoption of best practices for imaging and data curation will be an important step in advancing pollen analysis (Jaramillo et al. 2025). The initial investment can be high in terms of personnel time, equipment purchases, and data storage. However, public dissemination and long-term archival of image data support the mandate of many museums and research institutes and increase the societal value of their collections (Jaramillo et al. 2025).

With slide scanners that can scan an entire slide in under 1 hour and detection and classification models that can be trained in days (e.g., Punyasena et al. 2022; Theuerkauf et al. 2023), annotation remains the primary bottleneck in automated pollen analysis workflows. Continual learning—with human-in-the-loop annotations and iterative fine-tuning—allows models to improve as new images and new data are introduced. Confidence scores can be used to efficiently annotate false detections manually or using semi-automated methods. New annotations can be used to further fine-tune models, and these models can improve over time with expert feedback on model results. Strategies for effective human-in-the-loop data annotation are worth studying as a stand-alone problem, as for instance, Gimenez et al. (2024) has done for studying the effect of labeling specificity on model performance.

Finally, as foundation segmentation models like SAM-2 become incorporated into analysis workflows, procedures for detection and segmentation will become further streamlined. These foundation models can efficiently segment objects within an image with a single prompt (e.g., a mouse click, a coarse bounding box, or a coarse mask obtained from an upstream task), producing clean segmented images for training classification models. However, for palynological samples, trained detection models may still be needed to distinguish pollen and other specimens of interest from the diverse organic material that can be found on a palynological slide. However, once detected, foundation segmentation models are able to use a single set of coordinates to produce the clean contoured images needed for machine learning classification analyses.

Conclusions

Working in open-world scenarios means that we do not know a priori the full diversity that we will encounter in our analyses, so we need methodological approaches in which we continually improve both detectors and classifiers. Mixture-of-experts techniques, domain fine-tuning, and continual learning allow researchers to build upon shared generalized machine learning models, allowing each new generation of machine learning models to become more powerful than the last. The mixture-of-experts technique allows us to build models that are more resilient to changes in data distribution, and the small-grain detection described in our study is just one example of how the method can work with an unbalanced training dataset. Fine-tuning allows us to efficiently apply general models to new domains. These general models will also help annotate new data in new domains, using human-in-the-loop annotation to efficiently build large and diverse pollen image datasets. Developing automated analysis pipelines for fossil pollen analysis in the open world will mean adapting and continually updating the detection and classification models produced by the community to new

samples and new images. Data sharing and open-source software will play a vital role in creating the momentum needed to address the challenges of training models capable of handling the unique biases of fossil data.

Efficient object detection in scanned slide images will streamline the process of annotating and curating training data, and effective generalized detectors will lower barriers to the adoption of machine learning in palynology and other fields of microfossil research. While the underlying architecture of machine learning models may change, incorporating open-world methods will result in flexible and adaptable workflows that are accessible to all paleobiologists.

Acknowledgments. Thanks to K. Hagemans (formerly at Utrecht University) and T. van den Berg (University of Hull, formerly at Utrecht University) for preparing, annotating, and imaging the PAL IV samples; G. Dammers (Utrecht University) for his supervision in preparing the samples; D. Tcheng (formerly at the National Center for Supercomputing Applications, University of Illinois) for developing the MATLAB annotation script used for the PAL IV samples; and E. Bennink (Utrecht University) for modifications and updates to the annotation script. Funding for this research was provided by the University of Illinois Campus Research Board (grant RB22079 to S.W.P.), the University of Illinois School of Integrative Biology Francis M. and Harlie M. Clark Research Support Grant to J.T.F., the Dutch Research Council (NWO) (grant 824.14.018 to T.H.D.), and the Institute of Collaborative Innovation and the University of Macau (grant SRG2023-00044-FST to S.K.) and FDCT (grant 0067/2024/ITP2 to S.K.). This research was also supported in part by the Illinois Computes project through the University of Illinois Urbana-Champaign and the University of Illinois System. This work used the National Center for Supercomputing Applications' (NCSA) Delta computing platform, through allocation EES240072 from the Advanced Cyberinfrastructure Coordination Ecosystem: Services & Support (ACCESS) program, which is supported by U.S. National Science Foundation grants 2138259, 2138286, 2138307, 2137603, and 2138296 and the NCSA private cloud computing service Radiant. We thank associate editors A. Leslie and C. Stromberg and the reviewers for feedback that substantially improved the article.

Competing Interests. The authors declare no competing interests.

Data Availability Statement. Image stacks, annotation data, and trained detection models are archived through the Illinois Data Bank (Feng et al. 2025). We developed Python-based CLIs that are containerized using Docker for easy installation and provide many features like serial and parallel processing modes, storing output in different forms (folders or zip files), and optional parameters for customizing the runs of the applications and for interacting with the underlying software. The developed CLIs were successfully tested on MacOS (Apple M Chips and Apple Intel Chips) and NCSA's Delta HPC system using Apptainer. Source code for the described analysis (tagged with specific versions) is available on GitHub under Apache 2.0 open-source license at <https://github.com/paleopollen/ndpi-tile-cropper-cli/tree/v1.2.0> (Puthanveetil Satheesan et al. 2025a), <https://github.com/paleopollen/pollen-detection-cli/tree/v1.1.0> (Puthanveetil Satheesan et al. 2025b), and <https://github.com/paleopollen/post-processing-cli/tree/v1.0.0> (Puthanveetil Satheesan et al. 2025c). The original set of Jupyter Notebooks are available at: (https://github.com/paleopollen/open_world_pollen_detection).

Literature Cited

- Adhikari, B., and H. Huttunen. 2021. Iterative bounding box annotation for object detection. Pp. 4040–4046 in *25th International Conference on Pattern Recognition (ICPR)*, Milan, Italy. <https://doi.org/10.1109/ICPR48806.2021.9412956>.
- Akiba, T., T. Kerola, Y. Niitani, T. Ogawa, S. Sano, and S. Suzuki. 2018. PFDet: 2nd Place solution to Open Images Challenge 2018 Object Detection Track. <https://arxiv.org/abs/1809.00778>.
- Astolfi, G., A. B. Gonçalves, G. V. Menezes, F. S. B. Borges, A. C. M. N. Astolfi, E. T. Matsubara, M. Alvarez, and H. Pistori. 2020. POLLEN73S: an

- image dataset for pollen grains classification. *Ecological Informatics* **60**: 101165.
- Barnes, C. M., A. L. Power, D. G. Barber, R. K. Tennant, R. T. Jones, G. R. Lee, J. Hutton, et al. 2023. Deductive automated pollen classification in environmental samples via exploratory deep learning and imaging flow cytometry. *New Phytologist* **240**:1305–1326.
- Battiato, S., A. Ortis, F. Trenta, L. Ascari, M. Politi, and C. Siniscalco. 2020. Detection and classification of pollen grain microscope images. Pp. 980–981 in *Proceedings of the IEEE/CVF Conference on Computer Vision and Pattern Recognition Workshops (CVPR)*, Seattle, WA. <https://doi.org/10.1109/CVPRW50498.2020.00498>.
- Bendale, A., and T. Boulton. 2015. Towards open world recognition. Pp. 1893–1902 in *Proceedings of the IEEE Conference on Computer Vision and Pattern Recognition (CVPR)*, Boston, MA. <https://doi.org/10.1109/CVPR.2015.7298799>.
- Bourel, B., R. Marchant, T. de Garidel-Thoron, M. Tetard, D. Barboni, Y. Gally, and L. Beaufort. 2020. Automated recognition by multiple convolutional neural networks of modern, fossil, intact and damaged pollen grains. *Computers and Geosciences* **140**:104498.
- Buters, J., B. Clot, C. Galán, R. Gehrig, S. Gilge, F. Hentges, D. O'Connor, et al. 2022. Automatic detection of airborne pollen: an overview. *Aerobiologia* **40**:13–37.
- Campbell, I. D. 1999. Quaternary pollen taphonomy: examples of differential redeposition and differential preservation. *Palaeogeography, Palaeoclimatology, Palaeoecology* **149**:245–256.
- Cushing, E. J. 1967. Evidence for differential pollen preservation in late quaternary sediments in Minnesota. *Review of Palaeobotany and Palynology* **4**: 87–101.
- de Geus, A. R., C. A. Barcelos, M. A. Batista, and S. F. da Silva. 2019. Large-scale pollen recognition with deep learning. Pp. 1–5 in *27th European Signal Processing Conference (EUSIPCO)*, A Coruna, Spain. <https://doi.org/10.23919/EUSIPCO.2019.8902735>.
- Delcourt, P. A., and H. R. Delcourt. 1980. Pollen preservation and Quaternary environmental history in the Southeastern United States. *Palynology* **4**: 215–231.
- Duan, K., S. Bai, L. Xie, H. Qi, Q. Huang, and Q. Tian. 2019. CenterNet: keypoint triplets for object detection. Pp. 6568–6577 in *IEEE/CVF International Conference on Computer Vision (ICCV)*, Seoul, Korea. https://openaccess.thecvf.com/content_ICCV_2019/html/Duan_CenterNet_Keypoint_Triplets_for_Object_Detection_ICCV_2019_paper.html.
- Dunker, S., E. Motivans, D. Rakosy, D. Boho, P. Mäder, T. Hornick, and T. M. Knight. 2021. Pollen analysis using multispectral imaging flow cytometry and deep learning. *New Phytologist* **229**:593–606.
- Durand, M., J. Paillard, M.-P. Ménard, T. Suranyi, P. Grondin, and O. Blarquez. 2024. Pollen identification through convolutional neural networks: first application on a full fossil pollen sequence. *PLoS ONE* **19**:e0302424.
- Everingham, M., L. Van Gool, C. K. I. Williams, J. Winn, and A. Zisserman. 2010. The Pascal Visual Object Classes (VOC) Challenge. *International Journal of Computer Vision* **88**:303–338.
- Faegri, K. and J. Iversen. 1989. *Textbook of pollen analysis*. Fourth edition. by K. Faegri, P. E. Kaland, and K. Krzywinski. Wiley, Chichester, U.K.
- Feng, J. T., T. van den Berg, T. H. Donders, S. Kong, S. Puthanveetil Sathesan, and S. W. Punyasena. 2025. Slide scans, annotated pollen counts, and trained pollen detection models for fossil pollen samples from Laguna Pallcacocha, El Cajas National Park, Ecuador. Illinois Data Bank, University Library, University of Illinois at Urbana-Champaign. https://doi.org/10.13012/B2IDB-4207757_V1.
- Gimenez, B., S. Joannin, J. Pasquet, L. Beaufort, Y. Gally, T. de Garidel-Thoron, N. Combourieu-Nebout, et al. 2024. A user-friendly method to get automated pollen analysis from environmental samples. *New Phytologist* **243**: 797–810.
- Guo, R., C. Cui, Y. Du, X. Meng, X. Wang, J. Liu, J. Zhu, Y. Feng, and S. Han. 2019. 2nd Place solution in Google AI Open Images Object Detection Track 2019. <https://arxiv.org/abs/1911.07171>.
- Hagemans, K., C.-D. Tóth, M. Ormaza, W. D. Gosling, D. H. Urrego, S. León-Yáñez, F. Wagner-Cremer, and T. H. Donders. 2019. Modern pollen-vegetation relationships along a steep temperature gradient in the tropical Andes of Ecuador. *Quaternary Research* **92**:1–13.
- Hagemans, K., K. Nooren, T. de Haas, M. Córdova, R. Hennekam, M. C. A. Stekelenburg, D. T. Rodbell, H. Middelkoop, and T. H. Donders. 2021. Patterns of alluvial deposition in Andean lake consistent with ENSO trigger. *Quaternary Science Reviews* **259**:106900.
- Hagemans, K., D. H. Urrego, W. D. Gosling, D. T. Rodbell, F. Wagner-Cremer, and T. H. Donders. 2022. Intensification of ENSO frequency drives forest disturbance in the Andes during the Holocene. *Quaternary Science Reviews* **294**:107762.
- Hagemans, K., T. H. Donders, K. Nooren, I. E. E. Scheper, M. C. A. Stekelenburg, M. Theunissen, P. S. J. Minderhoud, et al. 2023. Anthropogenic activities in the páramo trigger ecological shifts in tropical Andean lakes. *Quaternary Research* **114**:18–29.
- He, K., X. Zhang, S. Ren, and J. Sun. 2016. Deep residual learning for image recognition. Pp. 770–778 in *Proceedings of the IEEE Conference on Computer Vision and Pattern Recognition (CVPR)*, Las Vegas, NV. <https://doi.org/10.1109/CVPR.2016.90>.
- Huang, Z., Z. Chen, Q. Li, H. Zhang, and N. Wang. 2020. 1st Place solutions of Waymo Open Dataset Challenge 2020—2D Object Detection Track. <https://arxiv.org/abs/2008.01365>.
- Jaramillo, C., S. W. Punyasena, D. de Alba, J. Bermudez, D. Caballero, K. Cardenas, D. Caro, et al. (2025) Digitizing collections to unlock the full potential of palynology. *Plants, People, Planet*, Special Issue, 1–16. <https://doi.org/10.1002/ppp3.70073>.
- Joseph, K. J., S. Khan, F. S. Khan, and V. N. Balasubramanian. 2021. Towards open world object detection. <https://arxiv.org/abs/2103.02603>.
- Kirillov, A., E. Mintun, N. Ravi, H. Mao, C. Rolland, L. Gustafson, T. Xiao, S. Whitehead, A. C. Berg, W.-Y. Lo, P. Dollár, and R. Girshick. 2023. Segment anything. <https://arxiv.org/abs/2304.02643>.
- Kong, S. 2022. aimerykong/pollenDetClsSystem: MEE-code-release-v1. Zenodo. <https://doi.org/10.5281/zenodo.6578814>.
- Kubera, E., A. Kubik-Komar, P. Kurasiński, K. Piotrowska-Weryszko, and M. Skrzypiec. 2022. Detection and recognition of pollen grains in multilabel microscopic images. *Sensors* **22**:2690.
- Langford, M., G. E. Taylor, and J. R. Flenley. 1990. Computerized identification of pollen grains by texture analysis. *Review of Palaeobotany and Palynology* **64**:197–203.
- Li, J., W. Cheng, X. Xu, L. Zhao, S. Liu, Z. Gao, C. Ye, and H. You. 2024. How to identify pollen like a palynologist: a prior knowledge-guided deep feature learning for real-world pollen classification. *Expert Systems with Applications* **237**:121392.
- Lin, T.-Y., M. Maire, S. Belongie, L. Bourdev, R. Girshick, J. Hays, P. Perona, D. Ramanan, C. L. Zitnick, and P. Dollár. 2014. Microsoft COCO: Common Objects in Context. <https://doi.org/10.48550/arXiv.1405.0312>.
- Linkert, M., C. T. Rueden, C. Allan, J.-M. Burel, W. Moore, A. Patterson, B. Loranger, et al. 2010. Metadata matters: access to image data in the real world. *Journal of Cell Biology* **189**:777–782.
- Liu, Z., Z. Miao, X. Zhan, J. Wang, B. Gong, and S. X. Yu. 2019. Large-scale long-tailed recognition in an open world. Pp. 2532–2541 in *Proceedings of the IEEE/CVF conference on computer vision and pattern recognition (CVPR)*, Long Beach, CA. <https://doi.org/10.1109/CVPR.2019.00264>.
- May, R. M. 1975. *Patterns of species abundance and diversity*. Pp. 197–227 in M. L. Cody and J. M. Diamond, eds. *Ecology and evolution of communities*. Harvard University Press, Cambridge, Mass.
- Menad, H., F. Ben-Naoum, and A. Amine. 2019. Deep convolutional neural network for pollen grains classification. *3rd Edition of the National Study Day on Research on Computer Sciences (JERI 2019)*, Saida, Algeria. *CEUR Workshop Proceedings* 2351. https://ceur-ws.org/Vol-2351/paper_34.pdf.
- Moy, C. M., G. O. Seltzer, D. T. Rodbell, and D. M. Anderson. 2002. Variability of El Niño/Southern Oscillation activity at millennial timescales during the Holocene epoch. *Nature* **420**:162–165.
- Nowlan, S., and G. E. Hinton. 1990. Evaluation of adaptive mixtures of competing experts. In R. P. Lippman, J. Moody, and D. Touretzky, eds. *Advances in Neural Information Processing Systems* **3**:774–780.
- Oteros, J., A. Weber, S. Kutzora, J. Rojo, S. Heinze, C. Herr, R. Gebauer, C. B. Schmidt-Weber, and J. T. M. Buters. 2020. An operational robotic pollen monitoring network based on automatic image recognition. *Environmental Research* **191**:110031.

- Padilla, R., W. L. Passos, T. L. B. Dias, S. L. Netto, and E. A. B. da Silva. 2021. A comparative analysis of object detection metrics with a companion open-source toolkit. *Electronics* **10**:279.
- Pan, S. J., and Q. Yang. 2010. A survey on transfer learning. *IEEE Transactions on Knowledge and Data Engineering* **22**:1345–1359.
- Platt, J. 1999. Probabilistic outputs for support vector machines and comparisons to regularized likelihood methods. *Advances in Large Margin Classifiers* **10**:61–74.
- Punyasena, S. W., D. S. Haselhorst, S. Kong, C. C. Fowlkes, and J. E. Moreno. 2022. Automated identification of diverse Neotropical pollen samples using convolutional neural networks. *Methods in Ecology and Evolution* **13**: 2049–2064.
- Puthanveetil Satheesan, S., J. Feng, S. Kong, and S. Punyasena. 2025a. A command line interface for NDPI format image tile cropping. <https://doi.org/10.5281/zenodo.15264408>.
- Puthanveetil Satheesan, S., J. Feng, S. Kong, and S. Punyasena. 2025b. A command line interface for pollen detection on z-stack images. <https://doi.org/10.5281/zenodo.15176855>.
- Puthanveetil Satheesan, S., S. Kong, and S. Punyasena. 2025c. A command line interface for basic post-processing of pollen detection images using Segment Anything Model 2 (SAM 2). <https://doi.org/10.5281/zenodo.15285826>.
- Ravi, N., V. Gabeur, Y.-T. Hu, R. Hu, C. Ryali, T. Ma, H. Khedr, et al. 2024. SAM 2: Segment Anything in images and videos. <https://arxiv.org/abs/2408.00714>.
- Ren, S., K. He, R. Girshick, and J. Sun. 2016. Faster R-CNN: towards real-time object detection with region proposal networks. *IEEE Transactions on Pattern Analysis and Machine Intelligence* **39**:1137–1149.
- Rostami, M. A., B. Balmaki, L. A. Dyer, J. M. Allen, M. F. Sallam, and F. Frontalini. 2023. Efficient pollen grain classification using pre-trained Convolutional Neural Networks: a comprehensive study. *Journal of Big Data* **10**:151.
- Sevillano, V., and J. L. Aznarte. 2018. Improving classification of pollen grain images of the POLEN23E dataset through three different applications of deep learning convolutional neural networks. *PLoS ONE* **13**:e0201807.
- Sevillano, V., K. Holt, and J. L. Aznarte. 2020. Precise automatic classification of 46 different pollen types with convolutional neural networks. *PLoS ONE* **15**:e0229751.
- Tešendić, D., D. Boberić Krstićev, P. Matavulj, S. Brdar, M. Panić, V. Minić, and B. Šikoparija. 2022. RealForAll: real-time system for automatic detection of airborne pollen. *Enterprise Information Systems* **16**:1793391.
- Tetard, M., R. Marchant, G. Cortese, Y. Gally, T. de Garidel-Thoron, and L. Beaufort. 2020. Technical note: a new automated radiolarian image acquisition, stacking, processing, segmentation and identification workflow. *Climate of the Past* **16**:2415–2429.
- Theuerkauf, M., N. Siradze, and A. Gillert. 2023. A trainable object finder, selector and identifier for pollen, spores and other things: a step towards automated pollen recognition in lake sediments. *The Holocene* **34**:297–305.
- Traverse, A. 2007. *Paleopalynology*, Vol. **28**. Springer Science and Business Media, Dordrecht, Netherlands.
- von Allmen, R., S. O. Brugger, K. D. Schleicher, F. Rey, E. Gobet, C. J. Courtney Mustaphi, W. Tinner, and O. Heiri. 2024. Method development and application of object detection and classification to Quaternary fossil pollen sequences. *Quaternary Science Reviews* **327**:108521.
- Wada, K., mpitid, M. Buijs, Zhang Ch. N., なるみ, Bc. Martin Kubovčík, A. Myczko, et al. 2021. wcentaro/labelme: v4.6.0. Zenodo. <https://zenodo.org/records/5711226>.
- Wang, Y., W. Yang, F. Ma, J. Xu, B. Zhong, Q. Deng, and J. Gao. 2020. Weak supervision for fake news detection via reinforcement learning. *Proceedings of the AAAI Conference on Artificial Intelligence, New York, NY* **34**(01): 516–523. <https://doi.org/10.1609/aaai.v34i01.5389>
- Wu, X., L. Xiao, Y. Sun, J. Zhang, T. Ma, and L. He. 2022. A survey of human-in-the-loop for machine learning. *Future Generation Computer Systems* **135**: 364–381.
- Zhang, Yu, Zhongyin Guo, Jianqing Wu, Yuan Tian, Haotian Tang, and Xinming Guo. 2022. Real-time vehicle detection based on improved YOLO v5. *Sustainability* **14**:12274.
- Zhou, Z., J. Shin, L. Zhang, S. Gurudu, M. Gotway, and J. Liang. 2017. Fine-tuning convolutional neural networks for biomedical image analysis: actively and incrementally. Pp. 4761–4772 in *Proceedings of the IEEE Conference on Computer Vision and Pattern Recognition*. <https://doi.org/10.1109/CVPR.2017.506>.
- Zhuang, F., Z. Qi, K. Duan, D. Xi, Y. Zhu, H. Zhu, H. Xiong, and Q. He. 2020. A comprehensive survey on transfer learning. Pp. 43–76 in *Proceedings of the IEEE*. <https://doi.org/10.1109/JPROC.2020.3004555>.